Soft Matter

PAPER

Screening and designing patchy particles for optimized self-assembly propensity through assembly pathway engineering

Eric Jankowski[a] and Sharon C. Glotzer*[b]

Self-assembly holds promise for creating new materials and devices because of its inherent parallelism, allowing many building blocks to simultaneously organize using preprogrammed interactions. An important trend in nanoparticle and colloid science is the synthesis of particles with unusual shapes and/or directional ("patchy") interactions, whose anisotropy allows, in principle, assemblies of unprecedented complexity. However, patchy particles are more prone to long relaxation times during thermodynamically driven assembly, and there is no *a priori* way of predicting which particles might be good assembly candidates. Here we demonstrate a new conceptual approach to predict this information using sequences of intermediate clusters that appear during assembly. We demonstrate our approach on a family of model building blocks as well as a real system of CdTe/CdS tetrahedra and find design rules for engineering the optimized assembly of target structures.

1 Introduction

Given a system of interacting particles, complex structures on macroscopic length scales can be synthesized *via* self-assembly when thermodynamics and kinetics favorably conspire.[1–5] As one example, the wires, sheets, helices, and colloidal crystals of supra-particles assembled from CdTe/CdS nano-tetrahedra[6–8] demonstrate the rich structural diversity accessible for a single type of building block. These nanoparticles hold promise for the assembly of materials with unique photonic, electronic, and mechanical properties,[9] as do colloids, DNA, and DNA-functionalized particles.[10–12] Finding the experimental conditions at which a set of building blocks robustly assembles any one ordered structure can require considerable effort and some amount of luck, and there is no guarantee that the assembled structure will find application. Finding a building block that will self-assemble a prescribed target structure with narrowly specified macroscopic properties is even more difficult because each specification can constrain the building block materials that can be used, possibly precluding self-assembly in any region of experimentally realizable state space.

In the case where candidate building blocks for self-assembly have already been identified it is in principle possible to create "phase diagrams" that map out thermodynamically stable equilibrium structures as a function of parameter space. In practice this is not a trivial task and much theoretical work has been devoted to the development of sophisticated computational techniques that allow for the equilibrium simulation of complex building blocks. Standard Monte Carlo (MC) simulation schemes have been extended in numerous ways to include special moves that allow for faster equilibration times of complex building blocks. Volume bias moves, coordinated cluster moves, and convex polyhedra overlap calculations have enabled the efficient simulation of patchy colloids, lattice tetrominoes, and hard tetrahedra.[13–17] Molecular dynamics (MD) simulations have also played an integral role in the prediction of self-assembled structures, and recent developments in GPU hardware architectures and algorithms have enabled the simulation of block copolymers, tethered nanoparticles, and arbitrary rigid bodies at longer time scales than ever before.[18–20] Unfortunately, when an equilibrium solution or simulation of patchy particles fails to generate an ordered pattern it is not always obvious whether the culprit is thermodynamics or kinetics. Recently there have been studies that attempt to quantify kinetic trapping through fluctuation-dissipation ratios,[21,22] and through the interplay between specific and nonspecific interactions,[3,5,23] but these methods do not provide predictive capabilities for thermodynamically stable structures.

The fact that both thermodynamics and kinetics can prevent a system of particles from self-assembling is particularly troublesome for experimentalists that search parameter space *via* trial-and-error because experiments that fail to assemble do not provide information about how assembly might be improved. In this work we propose a methodology (Fig. 1) for the rational design of building blocks optimized for self-assembly that focuses on *assembly pathway engineering*: identifying the traps that occur as a system assembles so they may be circumvented. As systems self-assemble we hypothesize that the

[a]Department of Chemical Engineering, University of Michigan, 2300 Hayward St., Ann Arbor, 48109, USA

[b]Department of Chemical Engineering and Department of Materials Science and Engineering, University of Michigan, 2300 Hayward St., Ann Arbor, 48109, USA. E-mail: sglotzer@umich.edu; Fax: (+734) 764-7453; Tel: (+734) 615-6296
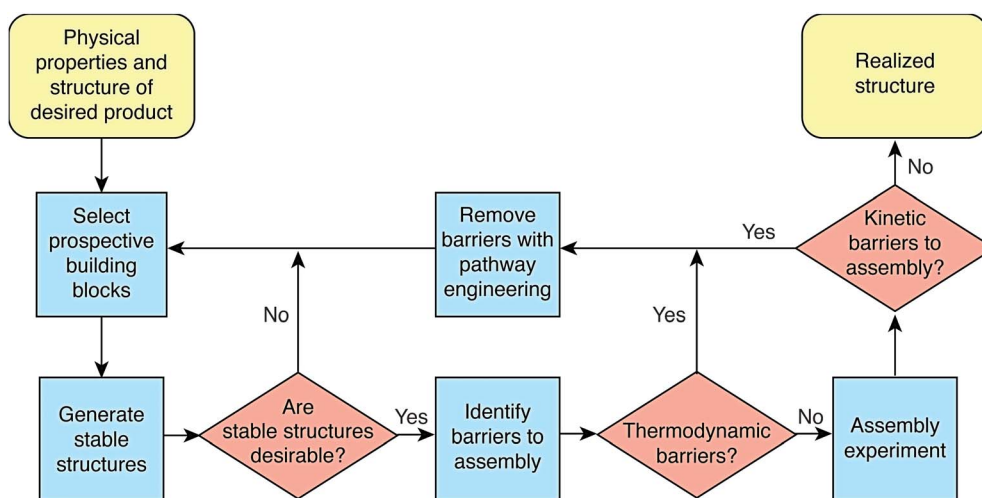
Fig. 1 Assembly pathway engineering algorithm. In this work we use BUBBA with shape matching to identify stable structures and thermodynamic barriers to assembly, and MC simulations as assembly experiments.[24] Perturbation-response methods,[21,22] molecular dynamics, and new shape matching techniques[25] will all play integral roles in assembly pathway engineering.

thermodynamically stable intermediate clusters that arise hold information about their ability to order. These sequences of intermediate clusters are *assembly pathways* and we propose a methodical analysis of them to predict the degree to which a system of building blocks will assemble a target pattern, which we refer to as the building block's *assembly propensity* for the pattern. We foresee assembly pathway engineering proceeding as a collaboration among structural identification, kinetic measurements, and the assembly pathway analysis described here. These components are indicated by the red diamonds in Fig. 1.

Our approach begins with the physical properties and structure of a product that we aim to create *via* self-assembly. The prospective building blocks that could be used are constrained both by the synthesis capabilities of a particular lab and the properties of the target product, *e.g.*, metallic nanoparticles should be avoided if an insulating material is desired. These building blocks are then screened using a thermodynamic method to generate stable structures. From the building blocks whose equilibrium structures are consistent with the target pattern we identify, *via* assembly pathway analysis, the traps that hinder self-assembly. We then modify the building blocks or the conditions under which they are assembled to optimize assembly, and finally perform experiments to test assembly rates. In principle any of a number of methods including MC or MD simulations could be employed to find thermodynamically stable structures or the intermediates that arise during assembly. In this work we use bottom-up building block assembly (BUBBA) for both.[15,24] Briefly, BUBBA is a computational tool that begins with a single building block and builds successively larger equilibrium structures hierarchically. To make a cluster of size N, BUBBA enumerates all possible combinations of pairs of clusters whose sizes sum to N, where each cluster in the pairing contributes non-negligibly to the ensemble of clusters for its size. In this way, BUBBA efficiently generates free-energy minimizing structures and the stable intermediates that lead to it, which we hypothesize govern assembly propensity.

The structure of this paper is as follows. First, we define and describe the computational methods and measurements we employ for assembly pathway engineering. Second, we consider model systems of patchy colloids and CdTe/CdS tetrahedra for which we test elements of our methodology. Third, we motivate the need for efficient structural screening tools by comparing the assembly propensities of seven model patchy colloids for a target structure. We find that assembly propensity can vary substantially from building block to building block, and show that assembly pathways provide predictive capabilities for assembly propensity. Fourth, we validate our pathway-based approach for a real system of CdTe/CdS tetrahedra. Fifth, we show the utility of BUBBA-informed pathway engineering by demonstrating ways thermodynamic traps can be avoided and by identifying the experimental conditions that maximize assembly. Finally, we discuss the limitations of our approach, highlighting the distinction between steric kinetic traps and interaction-based thermodynamic traps, and conclude with suggestions for further study.

2 Methods

The decision points represented by red diamonds in Fig. 1 can be, in principle, informed by any of a number of methods including, but not limited to, wet lab synthesis, Monte Carlo, molecular dynamics, simulated annealing, or mean field simulations. In this work we use Monte Carlo computer experiments to determine whether a target structure is kinetically accessible by a system of building blocks and we use BUBBA both for the screening of stable structures and for generating assembly pathways. The intermediate clusters generated with BUBBA are analyzed with shape-matching algorithms for consistency with target motifs, and assembly pathways are compressed into *pathway fingerprints* for clarity. Shape matching is also used to measure the degree to which a target structure has been assembled in Monte Carlo simulations.

2.1 Assembly pathways

For building blocks that undergo thermodynamically driven self-organization, an assembly pathway is a sequence of states that leads them from an initially disordered configuration to states that minimize free energy for the system as a whole.[23,26,27] These pathways can easily be generated for patchy particles with BUBBA, and we demonstrated the tradeoffs between efficiency, accuracy, and temperature in previous work.[24] In this work we consider pathways terminating at $N = 10$ building blocks and use a cutoff $c = 0.00001$ from ref. 24, ensuring enough clusters are included at each size to represent at least 99.999% of each partition function. The partition functions indicate which clusters are thermodynamically stable and the connectivities between partition functions indicate specific thermodynamically stable assembly pathways. An example assembly pathway generated with BUBBA for one of the patchy particles we study here is shown in Fig. 2a. Each blue box and red octagon in Fig. 2a is a node representing a cluster configuration, which is drawn near each node. The three numbers in each node represent the cluster's size, energy level (1 for lowest energy, 2 for second-lowest, *etc.*), and proportion of the partition function (out of 1.0) represented by that node at that size. The arrows connecting nodes indicate the cluster at the head can be created by combining the cluster at the tail with another cluster in the network, and the size of the arrowhead is proportional to the number of ways this pairing can be made. The color and shape of each node denotes whether or not the cluster is consistent (blue box) or inconsistent (red octagon) with a chosen target pattern, in this case the wide stripe motif in Fig. 3h.

2.2 Pathway fingerprints

In general, the assembly pathways for a building block at an arbitrary temperature are not as concise as Fig. 2a. The number of clusters that make up the partition function for a given N can grow up to many thousands for even small N, which makes pathway visualization in the style of Fig. 2a unwieldy. To visualize complicated assembly pathways in a way that makes them comparable to simple pathways we create assembly pathway "fingerprints" from the pathway data. The pathway fingerprint in Fig. 2b is an alternative and compact method of visualizing the cluster weight data from Fig. 2a at the cost of losing detailed path information. In a pathway fingerprint, each column represents an approximation of the partition function for clusters of a given
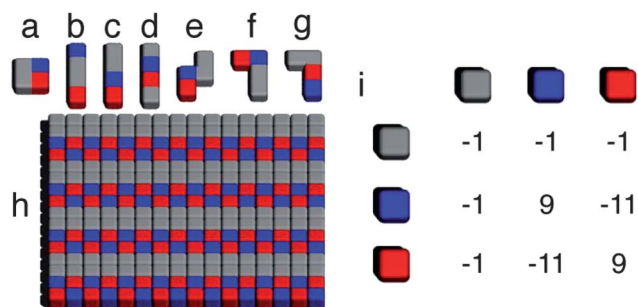

Fig. 3 a–g. Seven patchy particles from Troisi *et al.*,[13] h. Wide stripe motif that can be made by tiling a–g, predicted by BUBBA,[24] i. Interaction energies (units of ε) defined for neighboring subunits.
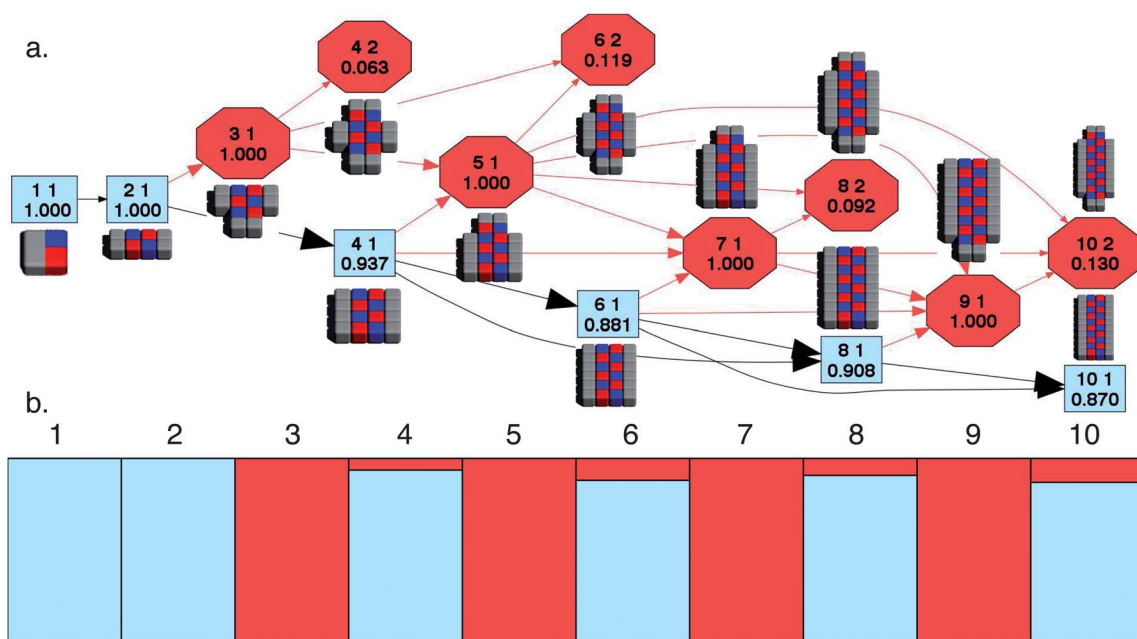

Fig. 2 a. The self-assembly pathways for patchy particle *a* from Fig. 3 at $k_BT/\varepsilon = 0.6$, from $N = 1$ to $N = 10$. Nodes indicate the size of a cluster, its energy level (1 for lowest, 2 for second-lowest, *etc.*), and its probability compared to clusters of the same size. Clusters are depicted near the nodes that represent them. Arrows connecting nodes indicate an assembly pathway, and the size of the arrowhead indicates the degeneracy of the pathway. Red nodes indicate clusters inconsistent with the wide stripe motif (3h). b. Assembly fingerprint created from the same data as in a. Each rectangle in a column represents a cluster and its height corresponds to its contribution to an N, V, T partition function. The proportion of red in a column indicates the probability of finding a cluster that is inconsistent with the target motif in an equilibrated N, V, T ensemble. With 100% red columns at $N = 3, 5, 7, 9$ we expect poor assembly of the wide stripe motif because all of these clusters are inconsistent with it.

size, increasing from one on the left to an arbitrary size on the right. Each cluster from a pathway becomes a rectangle in the fingerprint, whose height is proportional to the cluster's probability. As in the assembly pathways, target-motif-inconsistent clusters are indicated in red, and target-motif-consistent clusters are indicated in blue. To aid in visualization we omit the black border around a rectangle if the corresponding cluster's probability is less than 0.02.

2.3 Monte Carlo

We perform canonical ensemble (constant N, V, T) Monte Carlo (MC) simulations of patchy particles in order to assess the degree to which they self-assemble. Here, $N = 200$, $V = 2500$ (50×50 periodic lattice), and we consider instantaneous quenches to temperatures that are easily accessible in colloidal experiments.[28] All simulation runs are initialized with a random configuration of patchy particles, and we subsequently attempt 2×10^7 trial moves, requiring approximately two minutes of real time on a 2.8GHz Intel Core 2 Duo® processor. We quantify the degree to which a simulation snapshot assembles the wide stripe motif using a 2D Gaussian box filter, a standard technique in image shape matching.[25] We define the "motif match," for the ith subunit in a simulation snapshot as

$$m_i = \frac{1}{A} \sum_{j=-w}^{w} \sum_{k=-w}^{w} \delta(x_i + j, y_i + k) e^{-\frac{j^2 + k^2}{2\sigma}} \qquad (1)$$

where w is the box filter width, x_i and y_i are the coordinates of the ith subunit, and σ controls the width of the Gaussian kernel. We normalize m_i on [0, 1] with

$$A = \sum_{j=-w}^{w} \sum_{k=-w}^{w} e^{-\frac{j^2 + k^2}{2\sigma}} \qquad (2)$$

The delta function $\delta(x_i + j, y_i + k) = 1$ if the subunit located at $(x_i + j, y_i + k)$ in the simulation snapshot is the same type as the subunit in the wide stripe motif shifted (j, k) away from a reference cell, and $\delta(x_i + j, y_i + k) = 0$ otherwise, and will of course depend upon the orientation of the reference motif relative to the simulation snapshot. The reference cells of a motif are defined by their types, positions, and connectivity to other reference cells of the motif. The motif match for a simulation snapshot is defined as

$$M = \frac{1}{n} \sum_{i=0}^{n-1} \max(m_i \forall o) \qquad (3)$$

where n is the number of particle subunits, and only orientations o that maximize m_i are included in the sum. Here we use $\sigma = 2$ and $w = 2$ which results in M-values greater than 0.7 having a strong visual similarity to the reference motif, and $M < 0.6$ indicating a poor match.

3 Models

We demonstrate the generation and analysis of assembly pathways for a 2D system of patchy tetrominoes[13] and a 3D system of CdTe/CdS tetrahedra.[8] The assembly pathway analysis we present below is general for on-lattice and off-lattice systems in

2D and 3D as detailed in ref. 24. The seven patchy tetrominoes (Fig. 3a–g) we consider first are composed of two neutral (gray) subunits, one positive (red) subunit, and one negative (blue) subunit, and can rotate and translate on a 2D lattice. These seven tetrominoes are a subset of patchy tetrominoes studied previously, and share a common free energy minimizing motif (Fig. 3h) which was determined at $k_B T / \varepsilon = 0.1$ with BUBBA.[24] Inter-particle interaction energies are defined to model attractions and repulsions with relative magnitudes reminiscent of van der Waals, depletion, solvophobic, and/or charge–charge interactions. When two like-charged subunits share an edge, their resulting potential energy is $U = 9\varepsilon$, for opposite charges $U = -11\varepsilon$, and for a neutral subunit sharing a face with any other subunit type $U = -\varepsilon$.

We next validate the accuracy and utility of assembly pathway analysis on a system of CdTe/CdS tetrahedra with truncated tips whose surfaces are coated with thioglycolic acid stabilizers. Previously synthesized by Tang and Kotov,[6] and studied by Zhang et al.,[7] Srivastava et al.,[8] and Xia et al.[29] CdTe, CdSe, and CdS tetrahedra coated with DMAET or TGA stabilizers have been shown to have a rich phase space of self-assembled morphologies including wires, sheets, ribbons, helices, and colloidal crystals of spherical supra-particles. This richness arises from the complicated interactions between building blocks, including their shapes, van der Waals and hydrophobic attractions, hydrogen bonding, and electrostatics. This system admits straightforward analysis with BUBBA because the particle geometry and strong face-face interactions allow for a discretization of configuration space that enables iteration over all possible cluster pairings.

We consider CdTe tetrahedra whose intrinsic dipole moment is normal to one face as in ref. 8. We model long-range screened charge–charge interactions as well as charge–dipole and dipole–dipole interactions between tetrahedra using linear Debye–Hückel theory as in Phillies,[30] and add a constant surface potential for each pair of tetrahedral faces that are aligned as in Zhang et al.[7] The cluster degeneracies calculated by BUBBA for continuous systems require vibrational and rotational partition functions to be generated.[24] We assume the contribution of the vibrational partition function is identical for clusters of the same size, a valid assumption for these strongly-interacting particles that have been observed to fuse after assembly. This leaves the rotational partition function $Q_{rot} = B\sqrt{I}/s$ as the relevant contributor to entropy where B is a temperature-dependent constant that is identical for all clusters, I is the determinant of the inertial tensor, and s is the cluster's symmetry number.[24,31,32]

4 Assembly propensity

A system's ability to self-assemble a thermodynamically stable target pattern depends upon its path through phase space.[26,33] Experimental conditions such as density, temperature, solvent screening effects, quench rate, etc. all play a crucial role. A primary goal in self-assembly is the maximization of the assembly yield, the amount of desired product per unit of raw materials. It is therefore useful to define the "assembly propensity" as the degree to which the target pattern is achieved under the most optimal conditions. Given the seven patchy particles a–g in Fig. 3, which has the highest assembly propensity for the

wide stripe motif (Fig. 3h)? Just by looking at these particles it is not obvious that they share the same structure at low temperatures, nor is it obvious this structure minimizes free energy at higher temperatures. Further, it is not clear why any one of these particles should self-assemble the target motif in Fig. 3h more robustly than any other, or which one, if any, is the optimal candidate.

The average motif matches $\langle M \rangle$ for patchy particles a–g are generated using MC simulations and are shown as a function of temperature in Fig. 4. Each data point is the motif match averaged over the last 5×10^6 trial moves of 100 independent simulations, at 10,000 trial-move increments, with error bars denoting one standard deviation of the resulting distribution of M values. We define the self-assembly propensity P as the average value of $\langle M \rangle$ at the experimental conditions with the largest $\langle M \rangle$. It is clear from Fig. 4 that the seven particles from Fig. 3 have substantially different propensities, ranging from 0.48 for particle c up to 0.78 for particle b. We discern no obvious link between the shape of a particle's motif match profile and the particle's geometry or interaction anisotropy.

To explain the variance in assembly propensity and the difference in $\langle M \rangle$ *vs.* $k_B T/\epsilon$ for the seven patchy particles (Fig. 3a–g) studied here we consider assembly pathways which we generate with BUBBA.[24] At each stage in the assembly pathway we use shape matching[25] to identify clusters that are inconsistent with the wide stripe motif. Stages in the assembly pathway that are dominated by clusters inconsistent with a target motif are thermodynamic traps and a warning sign that a building block will not assemble robustly. As a case study we consider the assembly pathway fingerprints for patchy particles a and b, shown in Fig. 5 and 6, respectively. By visual inspection of the pathway fingerprints for these two building blocks, we expect lower assembly propensity for patchy particle a due to the prevalence of thermodynamic traps in its assembly pathways. Further, we see that for patchy particle a at $k_B T/\epsilon = 3.0$ there are more traps than at $k_B T/\epsilon = 0.8$, which is consistent with the lower average motif match measured at this state point (Fig. 5).
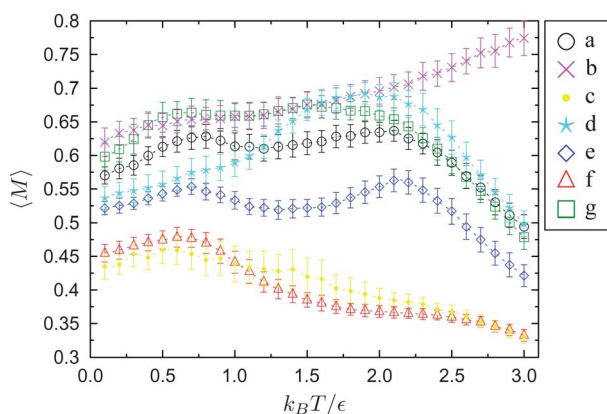

Fig. 5 Average wide stripe motif match for patchy particle a. Assembly pathway fingerprints and representative simulation snapshots are shown for $k_B T/\epsilon = 0.8$ and $k_B T/\epsilon = 3.0$. Decreased assembly propensity is correlated to increased proportion of red in an assembly fingerprint.

5 CdTe tetrahedra

We generate assembly fingerprints for CdTe/CdS tetrahedra to validate the utility of pathway analysis for an experimentally realized system. Keeping temperature constant, we use BUBBA to generate assembly pathways for the tetrahedra as functions of charge number q, dipole moment magnitude d (in units of Debye), and surface attraction. Here we constrain the search space to consider only combinations of neighboring tetrahedra whose faces are aligned, but allow the dipoles of each tetrahedron to point out any of the four faces. For particle charge of $+1e$ and dipole strength 100 we confirm the stability of single bilayer sheets found in ref. 6 and the double bilayer sheets found in ref. 8

Fig. 4 Average match to the wide stripe motif (Fig. 3h) as a function of temperature for the seven patchy tetrominoes from Fig. 3a–g. Error bars are one standard deviations of M averaged over 100 independent simulations for each data point. $\langle M \rangle > 0.7$ corresponds to a strong visual match and $\langle M \rangle < 0.6$ to very poor.
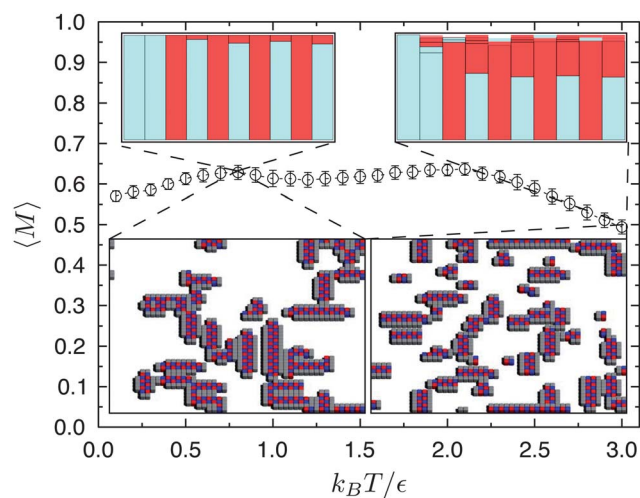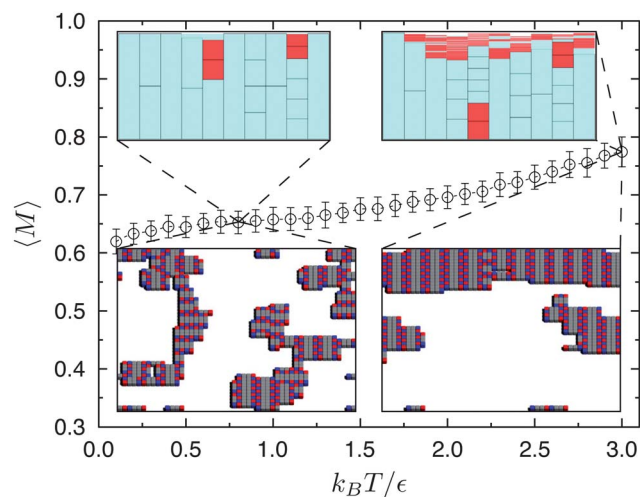

Fig. 6 Average wide stripe motif match for patchy particle b. Assembly pathway fingerprints and representative simulation snapshots are shown for $k_B T/\epsilon = 0.8$ and $k_B T/\epsilon = 3.0$. While the lower temperature assembly fingerprint appears superior, the shorter relaxation times and predominance of motif-consistent clusters at $k_B T/\epsilon = 3.0$ allow for better assembly.

(Fig. 7b) at $q = +3e$ and $d = 100$. Exploring the case of double-bilayer ribbons in more detail, we generate the assembly pathway fingerprint in Fig. 7d in three cpu-hours. For the double bilayer (Fig. 7a), we consider motif-inconsistent clusters to be all clusters that have tetrahedra on three or more layers, *e.g.*, Fig. 7c.

A full exploration of pathway sensitivity to charge strength, dipole strength, and surface charge is beyond the scope of the present work, but it is worth noting the complexity of the assembly pathways for these building blocks. At $N = 5$, over 6000 clusters contribute to the partition function, with no single cluster having a weight greater than 2%. For $N = 6$ there are several clusters that comprise a substantial proportion of the partition function, with many thousands of assembly pathways converging to these highest-weighted clusters. It is clear from the pathway fingerprint that not only are there many ways to combine clusters into a double bilayer (96% of the 104,396 clusters of size $N = 10$ are consistent with double bilayers), but also the proportion of out-of motif clusters at all calculated cluster sizes is low. This is expected from the ease with which the double bilayer ribbons are attained in experiments.
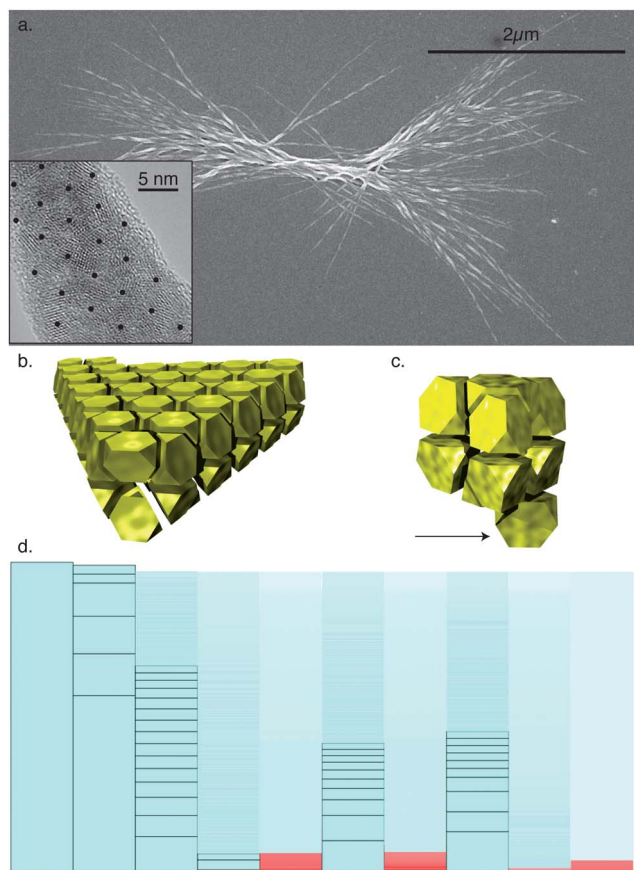
6 Screening and designing

The computational efficiency of assembly pathway generation coupled with structure identification is well suited for the screening of patchy particles. It can be used to identify the thermodynamically stable structures for a set of building blocks, as in ref. 24. After candidate building blocks for a motif are identified, such as the patchy tetrominoes and wide stripe motif studied here, assembly pathways can be generated at a range of experimental conditions to identify those with the greatest chance for robust assembly. Patchy particle 17 from Troisi *et al.* (shown inset in Fig. 8b) exemplifies the utility of screening temperatures for a building block that assembles a checkerboard motif. For reduced temperatures greater than $k_B T/\varepsilon = 1.0$, it is clear in Fig. 8a that the majority of clusters generated with BUBBA for $N = 3$–7 are inconsistent with the energy-minimizing checkerboard motif, implying that optimal self-assembly should occur for $0.1 \leq k_B T/\varepsilon \leq 1.0$. The motif match profile generated
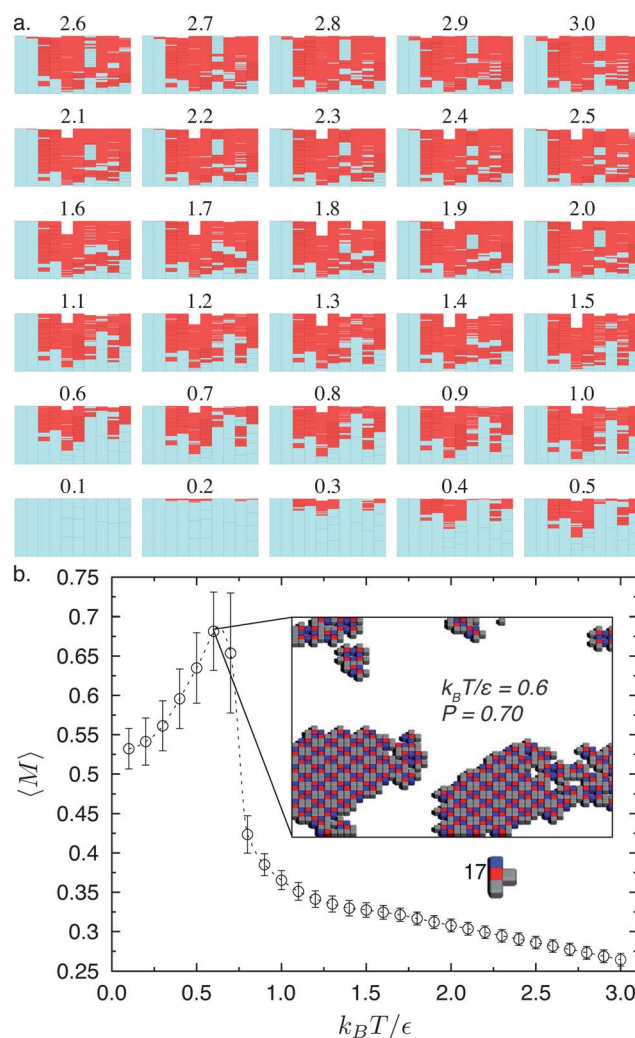

Fig. 7 a. TEM image of double bilayer ribbons that twist into helices from ref. 8. Inset shows a high-resolution image of a section of a ribbon with dots indicating approximate centers of co-planar tetrahedra. b. Double bilayer motif, $N = 100$ cluster predicted by BUBBA. c. Example out-of-motif $N = 10$ cluster, arrow indicates motif-breaking particle. d. Assembly pathway fingerprint for double bilayer-forming tetrahedra from ref. 8 with a charge of +3 and dipole moment of 100. Out-of-motif clusters have particles on more than two bilayers.

Fig. 8 a. Pathway fingerprints for patchy particle 17 for $0.1 \leq k_B T/\varepsilon \leq 3.0$. b. Motif match profile for patchy particle 17 with target motif and best-assembled snapshot inset. The motif match for this patchy particle is measured against a checkerboard reference structure that can be seen in the ordered central regions of the two large clusters in the inset snapshot.

with MC simulations in Fig. 8b confirms this hypothesis. The motif match jumps from $\langle M \rangle = 0.41$ at $k_B T/\varepsilon = 0.8$, to 0.57 at $k_B T/\varepsilon = 0.7$, is a maximum with $\langle M \rangle = 0.70$ at $k_B T/\varepsilon = 0.6$, and then drops to $\langle M \rangle = 0.60$ for $k_B T/\varepsilon = 0.5$. Thus, the quick generation (90 min for the 30 temperatures generated serially here, compared to 6000 cpu-hours for the MC simulations optimized with cluster moves) of pathway fingerprints with BUBBA permits the identification of state space where self-assembly is optimized. Efficient screening in this way is essential, as a naïve extrapolation of the data with $k_B T/\varepsilon > 1.0$ to low temperature would miss conditions with acceptable assembly.

Using shape-matching to identify motif-inconsistent clusters in assembly pathways we can determine patterns of traps that inform our pathway engineering strategies. One common pattern of trap shared across many of the patchy tetrominoes is the presence of motif-inconsistent clusters with odd-numbered sizes (*e.g.*, $N = 3, 5, 7, 9,...$). Patchy particle *a* exemplifies this pattern of traps (Fig. 5). These traps are caused by a single particle attaching to and breaking the symmetry of a desired cluster. In the case of patchy particle *a*, single-particle "caps" prevent further addition of particles to obtain wide stripes (Fig. 3h). This suggests that the $N = 2$ cluster may be a more effective building block candidate for self-assembly than the original particle because the same symmetry-breaking traps will be impossible to form. We perform this computer experiment by conducting Monte Carlo simulations at the same conditions as in Fig. 5, but where the 200 copies of particle *a* have been replaced by 100 copies of the $N = 2$ "mesoblock" which we denote *m2*. At the same temperature where patchy particle *a* assembles best with $\langle M \rangle = 0.66$, the mesoblock achieves $\langle M \rangle = 0.80$.

7 Discussion

We have performed assembly pathway fingerprint analysis for systems of patchy tetrominoes and truncated tetrahedra and demonstrated that there is a strong correlation between in-motif clusters in the assembly pathways of these fingerprints with favorable assembly propensity. There are three related ways in which comparisons between fingerprints presented here have not been perfectly correlated with assembly propensity measured by MC simulations at the same conditions. The first instance is the higher assembly propensity for patchy particle *b* at higher temperatures (Fig. 6), despite the presence of more motif-inconsistent clusters. The second is the drop in assembly propensity for particle 17 of ref. 24 when $k_B T/\varepsilon < 0.6$ (Fig. 8) despite the favorable-looking fingerprints. The third case is the imperfect assembly in Fig. 9 despite the perfect assembly fingerprint. All three cases are explained by assembly kinetics. For patchy particles *b* and 17, the thermodynamically preferred clusters generated by BUBBA show that larger proportions of the partition function are represented by in-motif clusters at low temperatures. At these low temperatures, however, the relaxation timescales are too long for robust assembly to occur. As BUBBA is a thermodynamic method, it does not predict regions of kinetic trapping, which highlights the important complementary contribution of the methods developed by Jack, Klotsa, Hagan, and Chandler.[21,22] The imperfect assembly of the mesoblock in Fig. 9 is also due to assembly kinetics. In this case the timescale of motif-consistent clusters agglomerating end-on rather than
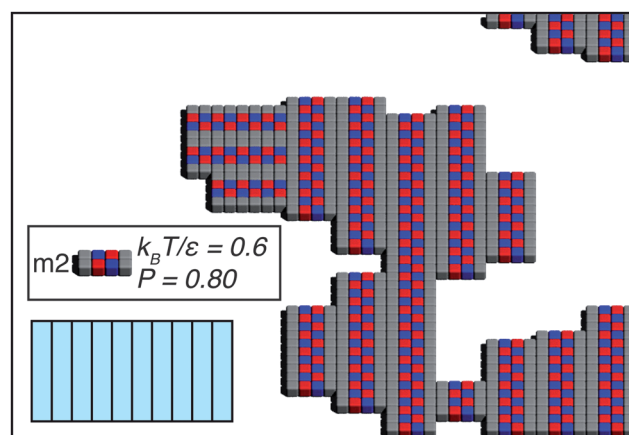

Fig. 9 Representative MC simulation snapshot for the $N = 2$ mesoblock made from patchy particle *a* at $k_B T/\varepsilon = 0.6$, the temperature with the maximum motif match as determined by MC simulations. The assembly pathway fingerprint at this temperature is inset, showing no thermodynamic traps for clusters with 10 or fewer building blocks.

perpendicular diverges as clusters grow in length. While this is unfortunate for this particular building block, it also provides a path forward for improved assembly, as it suggests that increasing the attraction between grey subunits might facilitate the wide stripe formation.

8 Conclusion

Through the use of assembly pathways, we have demonstrated that both model and real patchy particles can be efficiently screened for assembly propensity. We showed how building blocks designed to avoid particular barriers might assemble target patterns with higher propensity. We also showed how successive steps revealed in the assembly pathways could provide a blueprint for directed bottom-up assembly. Further, we showed that the fingerprint visualization of pathways is a useful tool in identifying thermodynamic conditions (such as temperature) that maximize self-assembly propensity. The computational efficiency of generating pathway fingerprints compared to experiments with unknown relaxation timescales makes it ideal for screening candidate building blocks and experimental conditions. Combining pathway-based screening techniques with assembly kinetics analysis we proposed a methodology for assembly pathway engineering which proceeds as in Fig. 1. We expect this method, its extensions, and alternative implementations to play a central role in the focused development of assembly engineering strategies.

References

1 G. M. Whitesides and B. Grzybowski, Self-assembly at all scales, *Science*, 2002, **295**(5564), 2418–2421.

2 Stephen Whitelam, Edward H. Feng, Michael F. Hagan and Phillip L. Geissler, The role of collective motion in examples of coarsening and self-assembly, *Soft Matter*, 2009, **5**, 1251–1262.

3 Stephen Whitelam, Control of pathways and yields of protein crystallization through the interplay of nonspecific and specific attractions, *Phys. Rev. Lett.*, 2010, **105**(8), 088102.

4 Thomas K. Haxton and Stephen Whitelam. Design rules for the self-assembly of a protein crystal. *arXiv:1110.5610v1* [*cond-mat.soft*], 2011.

5 James Grant, Robert L. Jack and Stephen Whitelam, Analyzing mechanisms and microscopic reversibility of self-assembly, *J. Chem. Phys.*, 2011, **135**(21), 214505.

6 Zhiyong Tang, Zhenli Zhang, Ying Wang, Sharon C. Glotzer and Nicholas A. Kotov, Self-assembly of CdTe nanocrystals into free-floating sheets, *Science*, 2006, **314**(5797), 274–278.

7 Zhenli Zhang, Zhiyong Tang, Nicholas A. Kotov and Sharon C. Glotzer, Simulations and analysis of self-assembly of CdTe nanoparticles into wires and sheets, *Nano Lett.*, 2007, **7**(6), 1670–1675.

8 Sudhanshu Srivastava, Aaron Santos, Kevin Critchley, Ki-Sub Kim, Paul Podsiadlo, Kai Sun, Jaebeom Lee, Chuanlai Xu, G. Daniel Lilly, Sharon C. Glotzer and Nicholas A. Kotov, Light-controlled self-assembly of semiconductor nanoparticles into twisted ribbons, *Science*, 2010, **327**(5971), 1355–1359.

9 Weijia Wen, Xianxiang Huang and Ping Sheng, Electrorheological fluids: structures and mechanisms, *Soft Matter*, 2008, **4**, 200–210.

10 Zhihong Nie, Alla Petukhova and Eugenia Kumacheva, Properties and emerging applications of self-assembled structures made from inorganic nanoparticles, *Nat. Nanotechnol.*, 2009, **5**(1), 15–25.

11 Fan Li, David P. Josephson and Andreas Stein, Colloidal assembly: the road from particles to colloidal molecules and crystals, *Angew. Chem., Int. Ed.*, 2011, **50**(2), 360–388.

12 Paul W. K. Rothemund, Folding DNA to create nanoscale shapes and patterns, *Nature*, 2006, **440**(7082), 297–302.

13 Alessandro Troisi, Vance Wong and Mark A. Ratner, An agent-based approach for modeling molecular self-organization, *Proc. Natl. Acad. Sci. U. S. A.*, 2005, **102**(2), 255–260.

14 Stephen Whitelam and Phillip L. Geissler, Avoiding unphysical kinetic traps in Monte Carlo simulations of strongly attractive particles, *J. Chem. Phys.*, 2007, **127**(15), 154101.

15 Eric Jankowski and Sharon C. Glotzer, A comparison of new methods for generating energy-minimizing configurations of patchy particles, *J. Chem. Phys.*, 2009, **131**(10), 104104.

16 Amir Haji-Akbari, Michael Engel, Aaron S. Keys, Xiaoyu Zheng, Rolfe G. Petschek, Peter Palffy-Muhoray and Sharon C. Glotzer, Disordered, quasicrystalline and crystalline phases of densely packed tetrahedra, *Nature*, 2009, **462**(7274), 773–777.

17 Alexander J. Williamson, Alex W. Wilber, Jonathan P. K. Doye and Ard A. Louis, Templated self-assembly of patchy particles, *Soft Matter*, 2011, **7**, 3423–3431.

18 Joshua A. Anderson, Chris D. Lorenz and A. Travesset, General purpose molecular dynamics simulations fully implemented on graphics processing units, *J. Comput. Phys.*, 2008, **227**(10), 5342–5359.

19 Carolyn L. Phillips, Christopher R. Iacovella and Sharon C. Glotzer, Stability of the double gyroid phase to nanoparticle polydispersity in polymer-tethered nanosphere systems, *Soft Matter*, 2010, **6**, 1693–1703.

20 Trung Dac Nguyen, Carolyn L. Phillips, Joshua A. Anderson and Sharon C. Glotzer, Rigid body constraints realized in massively-parallel molecular dynamics on graphics processing units, *Comput. Phys. Commun.*, 2011, **182**(11), 2307–2313.

21 Robert Jack, Michael F. Hagan and David Chandler, Fluctuation-dissipation ratios in the dynamics of self-assembly, *Phys. Rev. E: Stat., Nonlinear, Soft Matter Phys.*, 2007, **76**(2), 021119.

22 Daphne Klotsa and Robert L. Jack, Predicting the self-assembly of a model colloidal crystal, *Soft Matter*, 2011, **7**, 6294–6303.

23 Stephen Whitelam, Nonclassical assembly pathways of anisotropic particles, *J. Chem. Phys.*, 2010, **132**(19), 194901.

24 Eric Jankowski and Sharon C. Glotzer, Calculation of partition functions for the self-assembly of patchy particles, *J. Phys. Chem. B*, 2011, **115**(48), 14321–14326.

25 Aaron S. Keys, Christopher R. Iacovella and Sharon C. Glotzer, Characterizing structure through shape matching and applications to self-assembly, *Annu. Rev. Condens. Matter Phys.*, 2011, **2**(1), 263–285.

26 Michael F. Hagan and David Chandler, Dynamic pathways for viral capsid assembly, *Biophys. J.*, 2006, **91**(1), 42–54.

27 Jonathan P. K. Doye and Claire P. Massen, Characterizing the network topology of the energy landscapes of atomic clusters, *J. Chem. Phys.*, 2005, **122**(8), 84105.

28 W. B. Russel, D. A. Saville, and W. R. Schowalter. *Colloidal Dispersions*. Cambridge University Press: Cambridge, U.K., 1989.

29 Yunsheng Xia, Trung Dac Nguyen, Ming Yang, Byeongdu Lee, Aaron Santos, Paul Podsiadlo, Xhiyong Tang, Sharon C. Glotzer and Nicholas A. Kotov, Self-assembly of self-limiting monodisperse supraparticles from polydisperse nanoparticles, *Nat. Nanotechnol.*, 2011, **6**(9), 580–587.

30 George D. J. Phillies, Excess chemical potential of dilute solutions of spherical polyelectrolytes, *J. Chem. Phys.*, 1974, **60**(7), 2721–2731.

31 Donald A. McQuarrie. *Statistical Mechanics*. University Science Books: Sausalito, CA, 2000.

32 Guangnan Meng, Natalie Arkus, Michael P. Brenner and Vinothan N. Manoharan, The free-energy landscape of clusters of attractive hard spheres, *Science*, 2010, **327**(5965), 560–563.

33 Alex W. Wilber, Jonathan P. K. Doye, Ard A. Louis, Eva G. Noya, Mark A. Miller and Pauline Wong, Reversible self-assembly of patchy particles into monodisperse icosahedral clusters, *J. Chem. Phys.*, 2007, **127**(8), 085106.